Multi-Frequency Phase Difference of Arrival for precise localization in narrowband LPWA networks

Florian Wolf, Vincent Berg, Francois Dehmas, Valérian Mannoni, Sébastien de Rivaz

Multi-Frequency Phase Difference of Arrival for Precise Localization in Narrowband LPWA Networks

Florian Wolf, Vincent Berg, François Dehmas, Valérian Mannoni and Sébastien De Rivaz
Univ. Grenoble Alpes, CEA, Leti, F-38000 Grenoble, France
Email: {florian.wolf, vincent.berg, francois.dehmas, valerian.mannoni, sebastien.derivaz}@cea.fr

***Abstract*—In Low Power Wide Area (LPWA) networks, radio localization based on Time Difference of Arrival measurements has major benefits: energy consumption of the node and spectrum usage are contained. Temporal resolution and hence positioning accuracy is however limited by the bandwidth of the LPWA narrowband signals. Multi-channel ranging, that relies on multiple narrowband signals that are sequentially transmitted on different and discontinuous channels, has recently been proposed to improve precision. However, the concept has not been adapted yet to differential uplink localization techniques. This paper studies and proposes adaptations to multi-channel ranging called Multi-Frequency Phase Difference of Arrival (MF-PDoA) for this purpose. It analyzes the impact of imperfect synchronization on its performance and concludes that MF-PDoA is robust and well adapted to the LPWA scenario.**

***Index Terms*—Localization, LPWA network, MF-PDoA, frequency hopping, narrowband localization, phase synchronization**

I. Introduction

Low Power Wide Area (LPWA) networks are emerging communication technologies that enable wireless connectivity on a large variety of objects in the context of the Internet of Things (IoT). Long-range communication of both, proprietary (e.g. Long Range from Semtech (LoRA)) and standardized solutions (Narrow-Band IoT (NB-IoT)), is achieved thanks to low levels of receiver sensitivity obtained by low data rates and narrowband modulation schemes.

Wearable health monitoring is one example of a promising application of LPWA networks [1]. It allows to remotely monitor a patient and in case of an emergency (e.g. heart stroke) alert services to quickly react. LPWA radios are suited for these applications thanks to their small size, low-power and low-cost, while providing indoor and outdoor coverage. Localization of the patient is essential to facilitate the work of emergency services. Global Navigation Satellite System (GNSS) solutions are unsuitable because of extra energy consumption and unavailability for indoor operation. An energy efficient approach should derive position information from the same radio signal as used to transmit health-monitoring data. However, current approaches are not accurate enough to meet the requirements of the application [1].

Time of Arrival (ToA) based localization is bound by the signal bandwidth used to estimate ranging information [2]. This makes precise LPWA localization challenging and difficult to resolve in a multipath environment. Practical implementations and field trial measurements in LoRA networks typically achieve mean positioning errors of $200\,\mathrm{m}$ in an urban environment [3]. A new technique, called coherent multi-channel ranging, has therefore been proposed to significantly improve precision. It relies on multiple narrowband signals that are sequentially transmitted on different and discontinuous channels to virtually increase the bandwidth [4][5]. This technique, based on multiple phase measurements or Phase of Flight (PoF), significantly improves temporal resolution and ranging precision, while preserving the narrowband modulation necessary for long-range communication. The technique has been so far evaluated in two-way ranging scenarios, where elements (nodes or base-stations) sequentially perform a two-way packet exchange in order to remove absolute time synchronization constraints [4][5]. When LPWA base stations are strictly synchronized using e.g. GNSS time reference, Time Difference of Arrival (TDoA) is preferred as it does not require a bi-directional exchange and therefore preserves the energy of the IoT node and limits spectrum occupancy.

Application of TDoA positioning techniques to multi-frequency PoF ranging or Multi-Frequency Phase Difference of Arrival (MF-PDoA) is however not straightforward. MF-PDoA in the context of Radio-frequency identification (RFID) passive tags has already been considered and proved efficient [6]. However, Phase Difference of Arrival (PDoA) in this context considers perfect phase, frequency and time synchronization between distributed antennas leading to major simplifications because frequency and phase is generated from a single Radio Frequency (RF) source (i.e.: the RFID reader). Furthermore, only very short ranges are possible. Promising implementation of MF-PDoA in a short-range indoor context is considered in [7] using $2.4\,\mathrm{GHz}$ IEEE 802.15.4 PHY-layers, however, synchronization between access points is performed using a reference device transmitting from a known location. This transmission signal is time interleaved with the transmission of the devices to be located to avoid large synchronization drifts. This approach is not recommended for LPWA networks where frequency resources are scarce. Besides, $80\,\mathrm{MHz}$ bandwidth and ranges up to a few meters are considered in [7].

This paper evaluates and derives performance of coherent

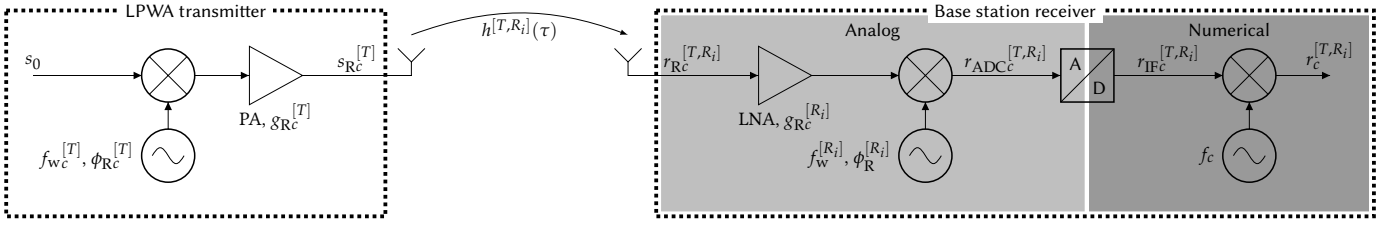

Fig. 1. Architecture model of the LPWA transmitter, channel model and base station receiver. Numerical stages of the base station are assumed coherent in phase.

multichannel ranging using a new MF-PDoA approach adapted to the LPWA scenario. A new phase synchronization mechanism imposes some architecture constraints on the base stations while significantly relaxing requirements on the nodes.

This paper is organized as follows. The system and signal model is introduced in Section II. The MF-PDoA estimator is presented in Section III. Section IV evaluates and compares performance of MF-PDoA with TDoA. Section V concludes the paper and outlines perspectives.

II. System and Signal Model

Range difference estimates between a transmitter T and multiple base stations R_i, $\Delta d^{[R_i,R_l]}$, are used by hyperbolic multilateration to derive the position of the transmitter. Position accuracy can be approximated as a product of range difference estimate standard deviation and geometric dilution of precision [8]. Hence, precise and accurate range difference estimates are key to achieve precise localization.

Multi-channel ranging relies on sequentially transmitting a narrowband signal, $s_0(t)$, over different frequencies $f_{\mathrm{w}c} = f_{\mathrm{w}} + f_c,\ c \in [0, C-1]$. The frequency, f_{w}, is called the central frequency and f_c, the channel frequency and is usually equal to $c\Delta f$. C is an integer equal to the number of channel frequencies considered by the algorithm.

In order to evaluate the quality of the localization metrics, a signal model with impairments is considered. The transmitter, channel and receiver architecture used to derive the signal model is given in Fig. 1. An arbitrary LPWA RF transmitter architecture is allowed on the node side, while on the base station, the reception stage is done through an Intermediate Frequency (IF) followed by a digital conversion and a second conversion stage performed digitally to keep coherence of phase between frequencies. It should be noted that this architecture model is compatible with cellular Internet of Things (IoT) base stations where receiver bandwidth is often much larger than a single channel.

Since transmitter and base stations are generally not synchronized with respect to the absolute reference time t, their local time may be expressed as:

$$t^{[X]} = \left(1 + \delta_f^{[X]}\right) t + t_0^{[X]}, \tag{1}$$

where $\delta_f^{[X]}$ is the normalized relative frequency offset of element $X \in \{T, R_i\}$. In the following and without loss of generalization, $\delta_f^{[T]}$ and $t_0^{[T]}$ are set to zero. As the localization scenario only considers one transmitter and multiple receivers, performance estimation of the ranging metrics may be done considering that the transmitter time is the reference time and imperfect synchronization of the receivers is relative to the transmitter time.

With these assumptions, when transmitted over carrier frequency $f_{\mathrm{w}c}$, the signal at the antenna of the IoT node becomes:

$$s_{\mathrm{R}c}^{[T]}(t) = g_{\mathrm{R}c}^{[T]}\, s_0\left(t - t_d^{[T]}\right) e^{j\left(2\pi f_{\mathrm{w}c} t + \phi_{\mathrm{R}c}^{[T]}\right)}, \tag{2}$$

where $g_{\mathrm{R}c}^{[T]}$, is a complex number value that models RF hardware gains, $t_d^{[T]}$, the time at start of transmission and $\phi_{\mathrm{R}c}^{[T]}$, an arbitrary phase term function of carrier $f_{\mathrm{w}c}$.

The RF signal is then transmitted over a wireless RF channel so that at base station R_i,

$$r_{\mathrm{R}c}^{[T,R_i]}(t) = s_{\mathrm{R}c}^{[T]}(t) * h^{[T,R_i]}(\tau) + \nu(t), \tag{3}$$

where $h^{[T,R_i]}(\tau)$ is the Channel Impulse Response (CIR) between transmitter T and base station R_i and is assumed stationary during the communication, $*$, the convolution product and $\nu(t)$, Additive White Gaussian Noise (AWGN).

Lets now assume that the coherence bandwidth of the channel, $h^{[T,R_i]}$, is significantly larger than the bandwidth of the baseband signal $s_0(t)$. This assumption allows to consider flat fading conditions for the transmitted signal $s_{\mathrm{R}c}^{[T]}(t)$, $c \in [0, C-1]$ and the convolution product in (3) can be replaced by a simple complex product.

$$r_{\mathrm{R}c}^{[T,R_i]}(t) = \alpha_c^{[T,R_i]} e^{j\varphi_c{}^{[T,R_i]}} s_{\mathrm{R}c}^{[T]}\left(t - \tau_0^{[T,R_i]}\right) + \nu(t), \tag{4}$$

where $\alpha_c^{[T,R_i]}$, $\varphi_c{}^{[T,R_i]}$ and $\tau_0^{[T,R_i]}$ are real numbers respectively equal to the amplitude, phase and delay of the channel at frequency $f_{\mathrm{w}c}$.

At the base station receiver, R_i, the received signal is amplified by a low noise amplifier, then mixed by $f_{\mathrm{w}}^{[R_i]} = (1 + \delta_f^{[R_i]}) f_{\mathrm{w}}$, to be downconverted to IF.

$$r_{\mathrm{ADC}c}^{[T,R_i]}(t) = g_{\mathrm{R}c}^{[R_i]}\, r_{\mathrm{R}c}^{[T,R_i]}(t) e^{-j\left(2\pi f_{\mathrm{w}}^{[R_i]} t + \phi_{\mathrm{R}}^{[R_i]}\right)} + \nu_{R_c}{}^{[T,R_i]}(t), \tag{5}$$

$$r_c^{[T,R_i]}[k] = g_{\mathrm{R}c}^{[T]}\, g_{\mathrm{R}c}^{[R_i]}\, \alpha_c^{[T,R_i]}\, \cdot s_0\left(\delta_{\mathrm{T}}^{[T,R_i]}\left(kT_{\mathrm{S}} - t_{\mathrm{A}c}^{[T,R_i]}\right)\right) \cdot e^{j\left(2\pi\delta_f^{[T,R_i]}(f_{\mathrm{w}}+f_c)kT_{\mathrm{S}} + \phi_{\mathrm{A}c}^{[T,R_i]}\right)} + n_c^{[T,R_i]}[k] \quad (8)$$

where $g_{\mathrm{R}c}^{[R_i]}$ is the complex gain of the receiver, $\phi_{\mathrm{R}}^{[R_i]}$, the unknown initial phase value of the receiver, and $\nu_{R_c}^{[T,R_i]}(t)$, noise $\nu(t)$ at the receiver IF. Signal $r_{\mathrm{ADC}c}^{[T,R_i]}(t)$ is then sampled every $kT_{\mathrm{S}}^{[R_i]}$ by the local clock of receiver R_i, where k is an integer:

$$r_{\mathrm{IF}c}^{[T,R_i]}[k] = r_{\mathrm{ADC}c}^{[T,R_i]}\left(\frac{kT_{\mathrm{S}} - t_0^{[R_i]}}{1+\delta_f^{[R_i]}}\right). \quad (6)$$

The samples are finally numerically down-converted to baseband with f_c such that $f_c + f_{\mathrm{w}} = f_{\mathrm{w}c}$.

$$r_c^{[T,R_i]}[k] = r_{\mathrm{IF}c}^{[T,R_i]}[k]\, e^{-j2\pi f_c kT_{\mathrm{S}}} + n_c^{[T,R_i]}[k], \quad (7)$$

where $n_c^{[T,R_i]}[k]$ is the equivalent AWGN noise at the baseband of receiver R_i.

The baseband received signal in (7) can finally be expressed as function of the baseband waveform $s_0(t)$ in (8) by combining (1) to (6). The following parameters are introduced:

1) Time dilation: Time dilation is a number close to 1 and accounts for relative sampling time errors between transmitter and receiver.

$$\delta_{\mathrm{T}}^{[T,R_i]} = \frac{1}{1+\delta_f^{[R_i]}} \quad (9)$$

2) Time of Arrival: the transmitted signal, $s_{\mathrm{R}c}^{[T]}$, is received at time, $t_{\mathrm{A}c}^{[T,R_i]}$, at base station R_i:

$$t_{\mathrm{A}c}^{[T,R_i]} = \left(1+\delta_f^{[R_i]}\right)\tau_0^{[T,R_i]} + t_0^{[R_i]} + \left(1+\delta_f^{[R_i]}\right)t_d{}^{[T]}\,. \quad (10)$$

3) Relative frequency offset: The received baseband signal at R_i is modulated by the remaining relative frequency offset, $\delta_f^{[T,R_i]}(f_{\mathrm{w}}+f_c)$, where:

$$\delta_f^{[T,R_i]} = \frac{-\delta_f^{[R_i]}}{1+\delta_f^{[R_i]}} \quad (11)$$

4) Phase of Arrival (PoA): The phase of arrival is a term dominated by the rotation of the carrier frequency over the duration of the time of arrival. Impairments on this term include relative frequency offset of the transmitter, the channel phase, $\varphi_c^{[T,R_i]}$, phase offsets due to time offsets between transmitter and receiver, as well as initial phase.

$$\begin{aligned}\phi_{\mathrm{A}c}^{[T,R_i]} &= -2\pi\left(f_{\mathrm{w}}+f_c\right)\tau_0^{[T,R_i]} + \varphi_c^{[T,R_i]} \\ &\quad + 2\pi\frac{\delta_f^{[R_i]}f_{\mathrm{w}} - f_c}{1+\delta_f^{[R_i]}}\, t_0^{[R_i]} \\ &\quad + \phi_{\mathrm{R}c}^{[T]} - \phi_{\mathrm{R}}^{[R_i]}. \end{aligned} \quad (12)$$

The latter term is particularly critical as it is the main limiting factor of quality of the MF-PDoA estimation process. The phase signal, $\phi_c^{[T,R_i]}[k]$, is then introduced as the phase of the received signal $r_c^{[T,R_i]}[k]$:

$$\phi_c^{[T,R_i]}[k] = 2\pi\delta_f^{[T,R_i]}\left(f_{\mathrm{w}}+f_c\right)kT_{\mathrm{S}} + \phi_{\mathrm{A}c}^{[T,R_i]}. \quad (13)$$

III. Range Difference Estimation

A. Multi-Frequency Phase Difference of Arrival (MF-PDoA)

The principle of MF-PDoA is based on the quasi linear relationship between phase $\phi_{\mathrm{A}c}$ and delay τ_0 in an homogeneous transmission medium (e.g. free space). Measuring the phase delay over multiple frequencies provides two main benefits: it improves range resolution and increases the maximum unambiguous range [4]. Range resolution is inversely proportional to the overall signal bandwidth while range ambiguity is inversely proportional to the frequency resolution. Fig. 2 gives an example of MF-PDoA spectrum occupation for an LPWA transmission. Packets of narrowband instantaneous bandwidth B are sequentially transmitted on C channels with channel spacing Δf. An overall virtual bandwidth $B_{\mathrm{virt}} = \Delta f(C-1)$ is therefore used.

MF-PDoA relies on a pair of base stations (R_i, R_l) to estimate the difference of PoAs from (12). As for TDoA, MF-PDoA constant but unknown terms in PoA are eliminated by the difference.

The PDoA measurement between the transmitter T and the pair of base stations (R_i, R_l) for channel c can be derived by subtracting (13) for both base stations:

$$\Delta\phi_c^{[R_i,R_l]}[k] = \phi_c^{[T,R_i]}[k] - \phi_c^{[T,R_l]}[k] \quad (14)$$

Eq. (14) can then be extended in details and analyzed.

$$\begin{aligned}\Delta\phi_c^{[R_i,R_l]}[k] &= -2\pi\left(f_{\mathrm{w}}+f_c\right)\left(\tau_0^{[T,R_i]} - \tau_0^{[T,R_l]}\right) && (15a)\\ &\quad + \varphi_c^{[T,R_i]} - \varphi_c^{[T,R_l]} && (15b)\\ &\quad - \left(\phi_{\mathrm{R}}^{[R_i]} - \phi_{\mathrm{R}}^{[R_l]}\right) && (15c)\\ &\quad - 2\pi\left(\frac{t_0^{[R_i]}}{1+\delta_f^{[R_i]}} - \frac{t_0^{[R_l]}}{1+\delta_f^{[R_l]}}\right)f_c. && (15d)\\ &\quad + 2\pi\left(\frac{\delta_f^{[R_i]}t_0^{[R_i]}}{1+\delta_f^{[R_i]}} - \frac{\delta_f^{[R_l]}t_0^{[R_l]}}{1+\delta_f^{[R_l]}}\right)f_{\mathrm{w}} && (15e)\\ &\quad - 2\pi\left(\frac{\delta_f^{[R_i]}}{1+\delta_f^{[R_i]}} - \frac{\delta_f^{[R_l]}}{1+\delta_f^{[R_l]}}\right)\left(f_{\mathrm{w}} + f_c\right)kT_s && (15f)\end{aligned}$$

1) Perfect base station synchronization: When the base stations are perfectly synchronized in both time and frequency, *i.e* $\delta_f^{[R_i]} = \delta_f^{[R_l]}$ and $t_0^{[R_i]} = t_0^{[R_l]}$, only the terms (15a), (15b) and (15c) remain. The base station IF

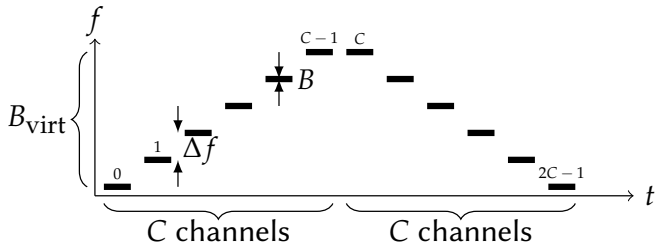

Fig. 2. Time versus frequency spectral representation of the transmitted MF-PDoA signal.

mixing architecture in Fig. 1 ensures phase coherence of the Local Oscillator (LO) during the entire MF-PDoA reception stage. Hence receiver phases $\phi_{\mathrm{R}}^{[R_i]}$ and $\phi_{\mathrm{R}}^{[R_l]}$ of (15c) are constant over all C channels. The term of interest $\tau_0^{[T,R_i]} - \tau_0^{[T,R_l]}$ can be estimated and (15c) has almost no impact on the range difference estimation.

2) Imperfect base station synchronization: In the more realistic case of imperfect synchronization between the base stations, e.g. when base stations are synchronized through GNSS signals [9], the time and frequency offset terms of (15) have to be considered. The inter-base station time synchronization offset $\Delta t_0 \approx t_0^{[R_i]} - t_0^{[R_l]}$ in (15d) directly impacts range difference measurement in (15), as it depends on the channel frequency f_c and is therefore generally not compensated for.

The term (15e), although directly impacted by the relative time and frequency errors $t_0^{[R_i]}$, $t_0^{[R_l]}$, $\delta_f^{[R_i]}$ and $\delta_f^{[R_l]}$, is independent from f_c and hence remains constant during the reception process. It thus has very little impact on the range difference estimation.

Finally, term (15f) is a phase rotation that is function of each channel c, the carrier frequency f_{w} and the channel frequency f_c. It is due to the relative Carrier Frequency Offset (CFO) between the base stations R_i and R_l. Although estimation of the CFOs, $\delta_f^{[R_i]}$ and $\delta_f^{[R_l]}$, is possible, the level of precision required is such that it would lie below the theoretical bound. This approach is therefore excluded. To compensate for this last term a symmetric frequency hopping scheme is thus introduced as illustrated in Fig. 2.

A frequency hopping scheme repeated with time reversal symmetry is thus considered (see Fig. 2). The time reversal symmetry imposes that the signal transmitted at time $t = kT_s$ is the same as the one at time $(N-k)T_s$. It is assumed that the duration of the narrowband signal s_0 is equal to N_cT_s. Every N_cT_s seconds, the carrier frequency of the signal is therefore changed. The overall C channels are covered in CN_cT_s seconds and the overall signal duration is equal to NT_s seconds, with $N = 2CN_c$. Besides, if at time $t_1 = kT_s$, the channel frequency of the narrowband signal is f_c, then it is also the channel frequency of the channel at time $t_2 = NT_s - t_1 = (N-k)T_s$ since channels are assumed stationary.

$\Delta\phi_c^{[R_i,R_l]}[k]$ and $\Delta\phi_c^{[R_i,R_l]}[N-k]$ are combined into a new variable $\Phi_c[k]$ assuming the property of time reversal in the transmitted sequence.

$$\begin{aligned}
\Phi_c[k] &= \Delta\phi_c^{[R_i,R_l]}[k] + \Delta\phi_c^{[R_i,R_l]}[N-k] \\
&= -4\pi\left(f_{\mathrm{w}} + f_c\right)\left(\tau_0^{[T,R_i]} - \tau_0^{[T,R_l]}\right) && \text{(16a)} \\
&\quad + 2\left(\varphi_c^{[T,R_i]} - \varphi_c^{[T,R_l]}\right) && \text{(16b)} \\
&\quad - 2\left(\phi_{\mathrm{R}}^{[R_i]} - \phi_{\mathrm{R}}^{[R_l]}\right) && \text{(16c)} \\
&\quad - 4\pi\left(\frac{t_0^{[R_i]}}{1+\delta_f^{[R_i]}} - \frac{t_0^{[R_l]}}{1+\delta_f^{[R_l]}}\right) f_c && \text{(16d)} \\
&\quad + 4\pi\left(\frac{\delta_f^{[R_i]} t_0^{[R_i]}}{1+\delta_f^{[R_i]}} - \frac{\delta_f^{[R_l]} t_0^{[R_l]}}{1+\delta_f^{[R_l]}}\right) f_{\mathrm{w}} && \text{(16e)} \\
&\quad - 2\pi\left(\frac{\delta_f^{[R_i]}}{1+\delta_f^{[R_i]}} - \frac{\delta_f^{[R_l]}}{1+\delta_f^{[R_l]}}\right)\left(f_{\mathrm{w}} \ + f_c\right) NT_s. && \text{(16f)}
\end{aligned}$$

Only term (16d) of (16) remains dependent of time as it changes every N_s symbols (i.e. every time the channel frequency is modified). This term is dependent on the synchronization between both receivers.

$\Phi_c[k]$ of (16) is then used to construct, $\tilde{H}_c$, a compound channel transfer function of the MF-PDoA system:

$$\tilde{H}_c = \mathcal{A}_c\, e^{j\Phi_c} = \left(H_c^{[T,R_i]}\right)^2 \left(\left(H_c^{[T,R_l]}\right)^2\right)^*, \qquad (17)$$

where $\mathcal{A}_c = \alpha_c^{[T,R_i]}\alpha_{2C-1-c}^{[T,R_i]}\alpha_c^{[T,R_l]}\alpha_{2C-1-c}^{[T,R_l]}$. The time domain equivalent of $\tilde{H}_c$ is the Compound CIR (CCIR), and may be derived by Inverse Discrete Fourier Transform (IDFT):

$$\tilde{h}(\tau) = \left(h^{[T,R_i]} * h^{[T,R_i]}\right) \otimes \left(h^{[T,R_l]} * h^{[T,R_l]}\right)(\tau), \quad (18)$$

were $\otimes$ is the cross-correlation product. The range difference $\Delta d^{[R_i,R_l]}$ is extracted by estimating the delay of the maximum amplitude in the CCIR of (18). The time reversal symmetry introduced in the transmitter to mitigate frequency error results in the auto-convolution of the CIR $h^{[T,R_i]}(\tau)$ and $h^{[T,R_l]}(\tau)$, while the cross-correlation product is introduced by the phase difference between transmitter and both base stations. This leads to unwanted path components in the CCIR and degrades the performance of estimation of the differential range.

B. Time Difference of Arrival (TDoA)

In comparison, the TDoA method estimates time difference of arrival from ToA estimates of (10). When base stations, (R_i, R_l) are synchronized, i.e. $t_0^{[R_i]} = t_0^{[R_l]}$ and $\delta_f^{[R_i]} = \delta_f^{[R_l]}$, the unknown and arbitrary transmitter time offset $t_0^{[T]}$ cancels and the resulting range difference is equal to

$$\Delta d^{[R_i,R_l]} = d^{[T,R_i]} - d^{[T,R_l]} = c_0\left(t_{\mathrm{A}}^{[T,R_i]} - t_{\mathrm{A}}^{[T,R_l]}\right). \quad (19)$$

Due to narrowband signals, ToA estimates t_{A} will not be as precise as MF-PDoA, but will serve as performance comparison to the proposed MF-PDoA technique.

IV. Performance Comparison between TDoA and MF-PDoA for LPWA IoT scenarios

Range difference derivations of Section III are used to evaluate and compare performance between TDoA and MF-PDoA for LPWA IoT scenarios. Two different LPWA scenarios have been considered for the evaluation: LoRA and NB-IoT. The conducted numerical MATLAB simulations assume AWGN channels. In the following, the Signal to Noise Ratio (SNR) level of the received signal has been considered identical for both receivers R_i and R_l. This is practically rarely the case, but constitutes a worst case scenario.

A. Cramer Rao Lower Bound (CRLB) for TDoA and MF-PDoA

The CRLB for MF-PDoA in presence of AWGN channel can be derived from the coherent multi-channel bound given in [10] where the CRLB is derived for PoA. MF-PDoA is a difference of two PoA metrics, $\phi_c^{[T,R_i]}$ and $\phi_c^{[T,R_l]}$, as defined in (14). Therefore the variance of the delay estimation of the difference of both phases is equal to the sum of the variances since $\phi_c^{[T,R_i]}$ and $\phi_c^{[T,R_l]}$ are uncorrelated. We can thus write:

$$\sigma_{\Delta\tau,CRLB}^{MF-PDOA} = \frac{1}{\sqrt{2\pi^2 \frac{E_s}{N_0} BW_{\mathrm{RMS}}^2}} \tag{20}$$

with root-mean-squared bandwidth

$$BW_{\mathrm{RMS}} = \sqrt{\frac{\int_{-\infty}^{+\infty} f^2 |S_0(f)|^2 df}{\int_{-\infty}^{+\infty} |S_0(f)|^2 df}} \tag{21}$$

and $\frac{E_s}{N_0}$, the symbol to noise power density over the transmitted sequence. Hence, under AWGN, the derivation of the CRLB of MF-PDoA is similar to the derivation of the CRLB of TDoA but with different values of $\frac{E_s}{N_0}$ and BW_{RMS}. CRLB however only considers performance with perfect synchronization. Numerical simulations are thus considered to compare performance of non perfectly synchronized receivers with the derived CRLB.

B. Application of MF-PDoA to LoRA numerology

For this application, one transmitter and two base stations are considered. The transmitted signal consists on a Gold code sequence of length $N_c = 32$ coded onto a Binary Phase Shift Keying (BPSK) modulation at the rate of 125kHz ($T_s = 8\mu$s). The transmitted sequence is repeated on $C = 16$ different frequencies with a channel spacing Δf equal to 200kHz and a time gap of 4 symbol periods (or 32μs). Time reversal symmetry is provided as shown in Fig. 2. The overall sequence duration is therefore less than 9.2ms. Simulations have considered arbitrary and independent carrier frequency errors of the receivers within $\pm 10\,\mathrm{ppm}$ relative to the transmitter. Carrier frequency error is compensated at the receiver by the Mengali algorithm [11].

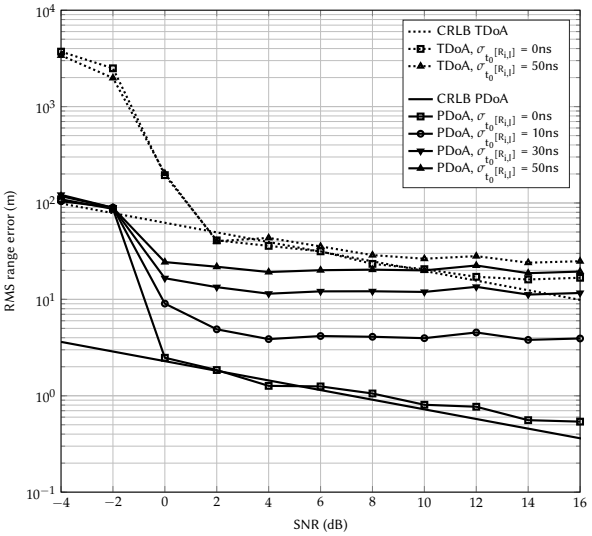

Fig. 3. LoRA scenario. Range difference error as a function of the SNR at the receiver and for different levels of synchronization errors $\sigma_{t_0^{[R_i,l]}}$.

Fig. 3 gives the standard deviation of the range difference error as a function of the SNR for the various simulated cases. The theoretical CRLB is also given for both TDoA and MF-PDoA. When perfect time synchronization between the base stations is considered, as expected, simulations converge towards CRLB for higher SNR levels and PDoA significantly outperforms TDoA. Although performance is limited by the carrier frequency estimator algorithm, the CRLB is reached. For a SNR of 6dB, the standard deviation error of MF-PDoA is equal to approximately 1m while the performance of TDoA is more than 30-times larger. Then time synchronization between receivers is relaxed. For each receiver, time synchronization errors are introduced using a normal distribution of increasing standard deviation, respectively 10ns, 30ns and 50ns on each receiver. For MF-PDoA, a performance floor is observed. This performance floor exactly matches the accuracy of the base station synchronization, as the performance floor converges towards $\sqrt{2}\sigma_{t_0^{[R_{i,l}]}} c_0$, where $\sigma_{t_0^{[R_{i,l}]}}$ is the standard deviation of the time synchronization error between base stations. When the synchronization error is set to 10ns (respectively 50ns), the RMS range error floor is equal to 4m (respectively 21m). Since TDoA performance is not as close to these limits, it only gets affected by synchronization errors at higher SNR values and only for the 50ns. The MF-PDoA behavior remains however very robust in presence of synchronization impairments.

C. Application of MF-PDoA to NB-IoT numerology

A second simulation scenario is geared towards application of MF-PDoA to NB-IoT. For this case, we assumed that signaling is transmitted over a Narrowband Physical Uplink Shared Channel (NPUSCH) modulated using a single carrier

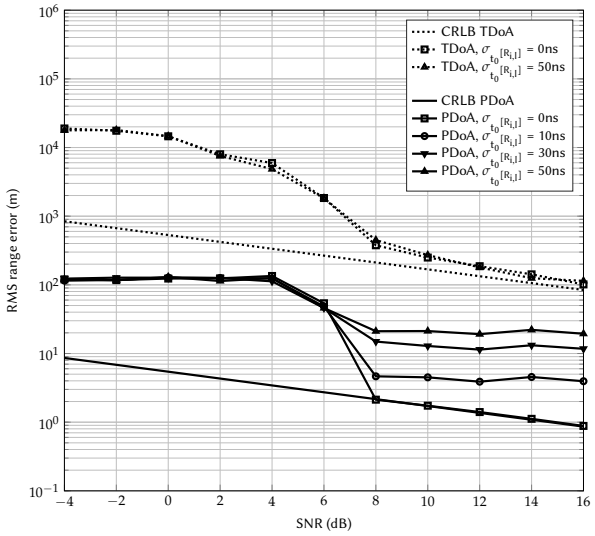

Fig. 4. NB-IoT scenario. Range difference error as a function of the SNR at the receiver and for different levels of synchronization errors $\sigma_{t_0^{[R_i,l]}}$.

modulation ($\pi/2$-BPSK) at a rate equal to 15kHz. The transmitted signal consists of a Barker sequence of $N_c = 7$ bits in order to fit the coded sequence within the duration of a NB-IoT frame slot. The transmitted sequence is repeated on $C = 16$ different frequencies with a channel spacing $\Delta f = 180$kHz. The complete localization signal could therefore be transmitted over two 15kHz single carrier NB-IoT frames (or 16ms). As for the LoRA simulations, the CRLB is estimated for this scenario. The carrier frequency error is set to ± 1 ppm as NB-IoT requires transmitter to synchronize within ± 0.2 ppm [12] and therefore receivers are not expected to compensate for large frequency errors. The carrier frequency error however requires compensation at the receiver and the Mengali algorithm is also used [11]. The time synchronization hypotheses are the same as for the previous scenario. It should be noted that although the numerology of NB-IoT has been carefully considered, frequency hopping is currently not supported by the standard and would require some amendments.

Fig. 4 gives the performance results for this scenario. Since the duration of the sequence is much shorter than in the previous case, performance of the TDoA and MF-PDoA algorithms converges for larger SNR values. For a SNR of 10dB, the standard deviation error of MF-PDoA is equal to approximately 2m while the standard deviation error of TDoA is equal to 150m. Floor performance behavior is the same as in the LoRA scenario when synchronization between transmitter and receivers is relaxed: when synchronization error is set to 10ns (respectively 50ns), the RMS range error floor is equal to 4m (respectively 21m). Both TDoA and MF-PDoA are robust to synchronization timing errors between receivers. However, since the signaling sequence is much shorter than in the previous application, MF-PDoA remains significantly better than TDoA. The TDoA performance is much worst (i.e. larger than 120m) than the error due to time synchronization (i.e. 21m).

V. Conclusion

This paper proposes and investigates an important evolution to coherent multi-channel ranging designed to limit energy consumption based on MF-PDoA for LPWA. The resulting metric provides difference in distances between the IoT node and two reference receivers (base stations) and provides localization with hyperbolic trilateration. As MF-PDoA relies on phase, time and frequency synchronization between base stations, the impact of imperfect synchronization between receivers is first analyzed and then simulated and compared against CRLB performance assuming perfect synchronization. Simulations performed for both LoRA and NB-IoT scenarios demonstrate the benefits of MF-PDoA in this context. Further work should consider field trial implementations of MF-PDoA with experimental hardware to confirm the hypothesis used for this simulation work.

Acknowledgment

This work was supported by the European Union's Horizon 2020 research and innovation programme under 5G-HEART project (grant agreement No 857034).

References

[1] P. H. Lehne *et al.*, "D3.1: Healthcare Vertical Trial Requirements Definition and Execution," 5GHEART deliverable, Tech. Rep., October 2019.

[2] M. Skolnik, *Radar Handbook*, 2nd ed. McGrawHill, 1990.

[3] N. Podevijn, D. Plets, M. Aernouts, R. Berkvens, L. Martens, M. Weyn, and W. Joseph, "Experimental TDoA Localisation in Real Public LoRa Networks," in *2019 International Conference on Indoor Positioning and Indoor Navigation (IPIN)*, 2019.

[4] F. Wolf, J.-B. Dore, X. Popon, S. de Rivaz, F. Dehmas, and J. P. Cances, "Coherent Multi-Channel Ranging for Narrowband LPWAN: Simulation and Experimentation Results," in *15th Workshop on Positioning, Navigation and Communications (WPNC)*, October 2018, pp. 1–6.

[5] F. Wolf, S. de Rivaz, F. Dehmas, V. Mannoni, V. Berg, and J. P. Cances, "Accurate Narrowband LPWA Ranging: Principles, Performance in AWGN and Multipath Channels," in *2020 European Conference on Networks and Communications (EuCNC)*, 2020, pp. 149–153.

[6] L. Qiu, Z. Huang, S. Zhang, C. Jing, H. Li, and S. Li, "Multifrequency Phase Difference of Arrival Range Measurement: Principle, Implementation, and Evaluation," *International Journal of Distributed Sensor Networks*, vol. 11, no. 11, p. 715307, 2015.

[7] M. Pichler, S. Schwarzer, A. Stelzer, and M. Vossiek, "Multi-Channel Distance Measurement With IEEE 802.15.4 (ZigBee) Devices," *IEEE Journal of Selected Topics in Signal Processing*, vol. 3, no. 5, pp. 845–859, Oct 2009.

[8] M. A. Spirito, "On the Accuracy of Cellular Mobile Station Location Estimation," *IEEE Transactions on Vehicular Technology*, vol. 50, no. 3, pp. 674–685, May 2001.

[9] LoRaAlliance, "Geolocation Whitepaper," https://lora-alliance.org/resource-hub/lora-alliance-geolocation-whitepaper, 2018, accessed: 2021/02/22.

[10] F. Wolf, C. Villien, S. de Rivaz, F. Dehmas, and J. P. Cances, "Improved Multi-Channel Ranging Precision Bound for Narrowband LPWAN in Multipath Scenarios," in *2018 IEEE Wireless Communications and Networking Conference (WCNC)*, April 2018, pp. 1–6.

[11] U. Mengali and M. Morelli, "Data-Aided Frequency Estimation for Burst Digital Transmission," *IEEE Transactions on Communications*, vol. 45, no. 1, pp. 23–25, Jan 1997.

[12] ETSI, *LTE; Evolved Universal Terrestrial Radio Access (E-UTRA); User Equipment (UE) radio transmission and reception (3GPP TS 36.101 version 14.3.0 Release 14)*, European Telecommunications Standards Institute (ETSI) Std., 2017.